Submitted to JCT, Oct. 2001

Optical Reflectance Of Metallic Coatings: Effect Of Aluminum Flake Orientation

Li-Piin Sung, Maria E. Nadal, Mary E. McKnight, Egon Marx
National Institute of Standards and Technology
Gaithersburg, MD 20899, USA
and
Brent Laurenti
Eckart America, Louisville, KY 40211, USA

Abstract

A set of aluminum-flake pigmented coatings having different flake orientations was prepared using various spray conditions. The orientations of individual flakes were determined from images obtained by laser scanning confocal microscopy. Reflectance measurements were carried out to quantify the optical properties of the coatings. A Gaussian orientation distribution or topographic map of the flakes was then used as input to a ray scattering model to calculate the optical reflectance of these coatings. The flake orientation distributions and the measured optical reflectance as a function of scattering angle are presented and the latter is compared to the calculated reflectance.

INTRODUCTION

Metallic coatings are the most popular exterior finish in the automotive industry and are widely used on other products such as cellular phones and biking helmets. The changes in lightness with illumination and viewing angles draw attention to the geometric features of these items.[1-3] A metallic finish consists of metallic flakes, typically aluminum (Al) flakes, in a polymer binder, which is often pigmented to create a different color appearance. Key characteristics that directly affect the optical properties of the metallic coatings are flake size, flake shape, flake surface roughness, spatial orientation of the flakes, flake concentration, and other pigments (additives). This paper will mainly address the effect of the flake orientation and, to some extent, flake surface roughness on the distribution of the light scattered by the coating. The flake orientation is strongly dependent upon the surface treatments of the flakes and the processing conditions.[1] Thus, it is crucial to be able to measure flake orientation accurately and to develop a methodology that can relate flake orientation to the optical properties of the materials. The methodology will provide support for control and prediction of appearance for product design, manufacture, and marketing.

Many efforts have been made to investigate the interrelation between formulation, processing, and spatial distribution of Al flakes in surface coatings and their appearance properties. A few studies[4-7] have included quantitative measurements of the flake orientation in cured coatings. Usually, flake orientation is determined using microscopy techniques applied to sectioned, cross-cut samples. This approach does not address directly the three-dimensional (3D) spatial orientation of the flakes. Recently, Kettler and Richter[7] used combined techniques of goniospectrophotometry, confocal laser scanning microscopy, and microscopy image analysis of cross-cut samples to obtain 3D orientation information. However, it is not obvious how one can deduce appearance properties from their orientation data.

A long-standing issue is how to characterize the flake orientation accurately and how to relate orientation information to optical properties. To tackle these problems quantitatively, we have implemented a methodology linking the flake orientation data to the optical properties by integrating measurements and modeling. Our methodology can be described as follows: (1) generation of topographic maps of the flakes in the coating using non-destructive laser scan-

ning confocal microscopy, (2) determination of the 3D spatial orientation distribution of the normals to the flakes from the topographic maps, (3) modeling of the link between flake orientation distribution and optical properties of the coating using a ray scattering model to calculate the optical reflectance, (4) alternatively, modeling of the direct link between topographic maps and optical reflectance, (5) measurement of the angular distribution of the light scattered by the coating, and (6) comparison of measured and calculated results. The inputs to the ray-scattering models are flake orientation distributions such as Gaussians of varying widths or topographic maps obtained with a confocal microscope. A preliminary report on this work was presented at a meeting.[8] Here we also show results of new measurements, we introduce corrections to the formulas that affect mainly scattering at large angles, and we include a new model that produces a scattering distribution from topographic maps.

EXPERIMENTAL

Materials

Two gray metallic pigmented coatings were prepared using a conventional hand-held spray gun. Each coating was applied to a black glass substrate with a smooth top clearcoat covering part of the surface. The coating consisted of an Al pigment in an acrylic-melamine polymer binder. The pigment was a special automotive grade that has a smooth surface finish and a platelet-like shape. The pigment loading level was 5% by mass fraction based on solid content of the coating and the average flake size was about 16 μm diameter and 1 μm thickness. We changed the coating appearance using the same composition by varying the amount of fluid allowed to pass through the spray gun. The samples were designated according to the position of the fluid control as 1-turn for normal operation and 1.5-turn for extra fluid output. The final dry

film thickness of samples was 38 μm ± 4 μm, measured by a Positector 6000 series coating thickness gauge.[a]

Visually, samples appeared lighter (of greater brightness) near the specular direction and became darker as the viewing angle moved away from this direction. The brightness difference between the two samples was small but visually detectable, and in the range of the rejection criteria for metallic coatings in an automotive processing line.

Microstructure Characterization

We used a Zeiss model LSM510[a] laser scanning confocal microscope (LSCM) to characterize the microstructure of the coatings. The LSCM uses coherent incident light and collects reflected or scattered light exclusively from a single plane, rejecting light out of the focal plane. The wavelength, numerical aperture (N.A.) of the objective, and the size of the collecting pinhole in front of the detector determine the resolution in the axial direction perpendicular to the surface.[9] In this study, an oil immersion objective (100×/1.3) was used. The scanning area of each confocal micrograph was about 92.1 μm × 92.1 μm at 0.18 μm/pixel, with a scanning time of 8 s/frame. The transverse and depth resolutions (point-to-point spread function) for an objective with a N.A. of 1.3 are 155 nm and 286 nm, respectively, for a scanning laser wavelength of 543 nm.

Figure 1a gives an example of a LSCM micrograph of an Al-pigmented coatings and the selected image of a single flake. LSCM micrographs consist of images of overlapping optical slices (a stack of z-scan images) with a 0.3-μm z-step. The size and orientation of an individual flake can be extracted and calculated from the topographic data as illustrated in Figure 1b; details will be presented later in the theory section.

---

[a] Certain instruments or materials are identified in this paper in order to adequately specify experimental details. In no case does it imply endorsement by NIST or imply that it is necessarily the best product for the experimental procedure.

Optical Reflectance Measurement

The in-plane bi-directional reflectance for two metallic pigmented samples was measured using the NIST spectral tri-function automated reference reflectometer (STARR).[10] The incident light flux was a collimated, monochromatic, polarized beam with a diameter of 14 mm and a bandwidth of 15 nm about a wavelength of 550 nm. Two rotation stages determine the incident angle of the beam on the sample and the viewing angle of the detector. Reflectance is calculated from the ratio of the reflected to the incident radiant flux. The incident flux is measured with the sample out of the beam path and the receiver positioned to accept the incident beam. The reflected radiant flux is measured with the sample in the beam path and the detector positioned at the desired angle. Figure 2 presents the optical geometry, where θ_o and θ_s are the incidence and scattering angles measured with respect to the normal of the sample. The sign convention is such that $\theta_s = -\theta_o$ indicates the specular reflection angle.

We measured the reflected intensity for incident angles of 0°, 30°, 45°, 60°, and 75°, using unpolarized incident light. Scattering angles with respect to the normal to the surface of the ranged from –70° to +70° at 0.5° increments. The expanded relative uncertainty for the reflectance data was 0.7 % ($k = 2$), calculated according to the procedures outlined in Ref. 9.

THEORY - RAY SCATTERING MODEL

The metallic flakes in our samples are significantly larger than the wavelength of light and tend to be oriented parallel to the coating surface. As a first approximation, we assume that the flakes are smooth, flat, and perfectly conducting, and we ignore multiple reflections. The angular distribution of the light scattered by the flakes can then approximately be determined from ray reflection by the flake surface.

Roughness of the coating surface and flake surface also causes diffuse scattering. In a first model, we assume that the flakes are flat and that the orientation of the flakes is the only cause of the scattering of light by the sample. A second model uses topographic maps of the flake surfaces in the interior of the coating obtained by the confocal microscope to determine the reflectance, thus including the surface roughness in the computations.

We first show how the ray is refracted at the coating surface and reflected by the flake surface, relating the incident direction, the normal to the flake surface and the scattered direction, which applies to both models. We then show how the assumed or measured distribution of the flake normal is defined and how it is used in the first model to compute the reflectance. Finally, we show how the reflectance is computed using flake surface topography in the second model.

Determination of the Path Followed by a Ray

We chose a coordinate system with the *z*-axis perpendicular to the average plane of the surface, so that the normal to the surface is $\hat{e}_z$, and with the *x*-axis in the plane of incidence. We designate by $\hat{n}$ the unit normal to a flake, which has Cartesian components n_x, n_y, and n_z, or spherical coordinates θ_n and φ_n.

The path followed by the incident ray as it is refracted at the surface of the coating, then reflected by a metallic flake, and then refracted again as it exits the coating is shown in Figure 3. If the instrument is restricted to take measurements in the plane of incidence and if we neglect the size of the aperture, we can ignore the dependence of the scattering on the azimuthal angle φ.

The incident beam comes in along the *xz*-plane in the direction defined by the angle θ_0. This beam is refracted into the coating where it propagates in the direction $\hat{k}'$ at an angle θ_0'. The angle θ_0' is determined by Snell's law, that is, $n\sin\theta_0' = \sin\theta_0$, where n is the real index of refraction of the coating. The intensity of the refracted beam is determined by the Fresnel coefficients, which depend on the polarization of the incident field. If θ_0 is fixed and only the intensity of the outgoing beam relative to that in the specular direction is used in the analysis, such constants can be ignored.

The ray is then specularly reflected by the flake in the direction $\hat{k}''$, assuming that Al flakes are perfect conductors, and refracted again at the boundary of the coating into the direction $\hat{k}'''$. If we restrict ourselves to the plane of incidence, the corresponding angles of the propagation vectors are related again by Snell's law, which in this case implies that $\sin\theta''' = n\sin\theta''$.

The polar angle θ''' then is the scattering angle θ_s. The refracted ray is not necessarily in the plane of incidence and the azimuthal angles satisfy $\varphi''' = \varphi'' = \varphi$. The normal to the flake is determined by

$$\hat{k}'' = \hat{k}' - 2\hat{k}' \cdot \hat{n}\hat{n} \quad \Rightarrow \quad \hat{n} = (\hat{k}'' - \hat{k}') \Big/ \left|\hat{k}'' - \hat{k}'\right|, \tag{1}$$

and either can be used to determine θ_n and φ_n.

The factor γ that determines the projection of the area perpendicular to the beam incident to the flake is the cosine of the angle between the normal to the flake and the direction of the incident beam in the substrate, that is,

$$\gamma(\theta_n, \varphi_n, \theta_0) = -\hat{n} \cdot \hat{k}' = (1 - \hat{k}'' \cdot \hat{k}')(2 - 2\hat{k}'' \cdot \hat{k}')^{-1/2} = [(1 - \hat{k}' \cdot \hat{k}'')/2]^{1/2}. \tag{2}$$

We can thus follow a ray from the incident direction to the outgoing direction when the normal to the flake surface is known. Alternatively, we can determine the direction of the normal to the flake that sends the ray into a particular outgoing direction.

Distribution of the Normals to the Flakes

We assume that the distribution of the orientation of the flakes is independent of the azimuthal angle, φ_n, and of the size of the flake. Since the intensity of the light scattered in a given direction is proportional to the total surface exposed at a given angle, the determination of the distribution of the normal has to take into account the size of the flakes instead of just the number of flakes. We call $p_2(\theta_n, \varphi_n)\mathrm{d}\Omega$ the probability that the normal direction lies within a solid angle $\mathrm{d}\Omega$ about θ_n and φ_n. Then, if $p(\theta_n)\mathrm{d}\theta$ is the probability that the polar angle lies within an angle $\mathrm{d}\theta$ about θ_n, we have

$$p(\theta_n)\mathrm{d}\theta = \int_0^{2\pi} p_2(\theta_n, \varphi)\sin\theta_n \mathrm{d}\varphi \mathrm{d}\theta = 2\pi\, p_2(\theta_n, 0)\sin\theta_n \mathrm{d}\theta. \tag{3}$$

We do not expect the function $p_2(\theta_n, \varphi_n)$ to diverge on the polar axis, so that *p(0)* vanishes and we work with a modified distribution function

$$\tilde{p}(\theta_n) = p(\theta_n)/\sin\theta_n, \tag{4}$$

assuming that the limit of the fraction is finite as $\theta_n \to 0$.

We determine $p(\theta_n)$ from confocal microscopy measurements, as shown in Figure 1. Our confocal microscope can determine the *z*-coordinate of the surface of a flake as a function of position, that is, $z(x, y)$ can be measured experimentally. If the surface is a plane, its equation has the form

$$\hat{n} \cdot \vec{x} = h \quad \Rightarrow \quad z = -(n_x/n_z)x - (n_y/n_z)y + h/n_z = ax + by + c\,. \tag{5}$$

The microscope gives coordinates along lines of constant x or constant *y*; in particular, we obtain the coordinates at the beginning and at the end of such a line. If they are (x_1, z_1) and (x_2, z_2) for a line of constant *y*, and (y_1', z_1') and (y_2', z_2') for a line of constant *x*, as shown in Figure 1b, the angles θ_x, θ_y, and θ_n are given by

$$\tan^2\theta_x = \zeta_x^2 = \left(\frac{z_2 - z_1}{x_2 - x_1}\right)^2, \quad \tan^2\theta_y = \zeta_y^2 = \left(\frac{z_2' - z_1'}{y_2' - y_1'}\right)^2, \quad \tan^2\theta_n = \zeta_x^2 + \zeta_y^2. \tag{6}$$

An estimate of the area of the flake can be obtained from

$$S \propto (x_2 - x_1)(y_2' - y_1')/(\cos\theta_x \cos\theta_y). \tag{7}$$

We thus find the distribution of the flake orientation by computing θ_n from Eq. (6) and adding a contribution equal to the area in Eq. (7) to the corresponding bin.

Barrick[11] has addressed a related problem — the connection between the angular distribution of scattered light and the slope and curvature distributions of a rough surface. He defines a probability density that we designate by $P_2(\zeta_x, \zeta_y)$, ignoring the dependence on higher-order derivatives. If the surface is isotropic, P_2 depends only on $\zeta = \tan\theta_n = (\zeta_x^2 + \zeta_y^2)^{1/2}$. To compare results, we relate the distribution $P(\zeta) = 2\pi\zeta P_2(\zeta_x, \zeta_y)$ to ours and find

$$\tilde{p}(\theta_n) = P(\tan\theta_n)/(\sin\theta_n \cos\theta_n). \tag{8}$$

This equation differs from Eq. (9) in Ref. 8 because we now believe that the distribution used by Barrick gives the slopes for a point selected at random in the xy-plane instead of the surface.

Light Scattering Distribution from Probability Densities for the Normal to the Flakes

To connect a distribution of the normals to the flakes to measurements made with an instrument we integrate over the angular aperture of a detector, given by the half-angle α. We assume that the *j*th detector, or the *j*th position of a single detector, is located in a direction given by the spherical coordinates ϑ_j and φ_j, $j = 1, ..., N$. If all the light reflected by the metallic flakes in a particular direction is collected by the detector in that direction, the intensity of the light scattered is proportional to the probability that the normal to the flake be oriented so that the light is reflected into the detector from the incident beam. The part of the incident beam that is reflected by a flake is then proportional to total flake area projected onto a plane perpendicular to the beam. To obtain the intensity, up to a factor, of the light scattered into the *j*th detector we have to integrate the probability distribution over the detector aperture $\Delta\Omega$,

$$I_j(\theta_0) = \int_{\Delta\Omega(\vartheta_j,\varphi_j)} \mathrm{d}\Omega'''(\cos\theta''/\cos\theta''')T_{av}(\theta'',\theta''')p'''(\theta''',\varphi''';\theta_0), \tag{9}$$

where p''' is the probability density of getting an outgoing ray in the $\hat{k}'''$ direction and T_{av} is the average transmittance obtained from those of a given polarization,[12]

$$T_{av} = \frac{\sin(2\theta'')\sin(2\theta''')[1+\cos^2(\theta''-\theta''')]}{2\sin^2(\theta''+\theta''')\cos^2(\theta''-\theta''')}. \tag{10}$$

This transmittance takes into account the flow of energy perpendicular to the surface; to consider the flow in the direction of the rays we have multiplied T_{av} by the ratio of the cosines of the angles in the integrand in Eq. (9).

Different probability densities are connected by conservation of probability, which involves changes in the element of solid angle expressed in terms of the Jacobian. To take into account the refraction of the outgoing ray at the dielectric boundary, we relate p''' to the corresponding probability density p'' in the coating by

$$p'''(\theta''',\varphi''';\theta_0) = p''(\theta'',\varphi'';\theta_0)(\cos\theta'''/n^2\cos\theta''). \tag{11}$$

We now relate this probability density to that of the normal to the flake. We find that

$$p''(\theta'',\varphi'';\theta_0) = \gamma(\theta_n,\varphi_n,\theta_0)J_n(\theta_n,\varphi_n;\theta'',\varphi'')\,p(\theta_n)/(2\pi\sin\theta''), \tag{12}$$

where the partial derivatives in the Jacobian J_n can be obtained from the first relation in Eq. (1) when spherical coordinates are used to express the unit vectors.

The integral in Eq. (9) then changes to

$$I_j(\theta_0) = \int_0^{\alpha} \sin\bar{\theta}\,\mathrm{d}\bar{\theta} \int_0^{2\pi} \mathrm{d}\bar{\varphi}\, \frac{\sin\theta_n}{2\pi n^2 \sin\theta''} T_{av}(\theta'',\theta''')\gamma(\theta_n,\varphi_n,\theta_0) J_n(\theta_n,\varphi_n;\theta'',\varphi'')\tilde{p}(\theta_n), \quad (13)$$

where the normal to the flake has to be found as a function of the new coordinates $\bar{\theta}$ and $\bar{\varphi}$ about a polar axis that corresponds to the center of the detector. We note that the Jacobian has factors that cancel the ratio of sine functions, that is, the solid angle elements are not deformed by this transformation.

If the integrand varies significantly over the region of integration, the integral in Eq. (13) is best evaluated numerically. A spherical cap of angle θ_c is defined around the axis of the detector and its contribution should be computed separately. If the integrand changes little across the solid angle, we can assume that it is a constant.

Figure 4 shows the calculated intensity distribution (reflectance normalized to 1 in the specular direction) at two incident angles as a function of scattering angle for two Gaussian modified angle distribution functions, $\tilde{p}(\theta_n)$, with half-widths $w = 4°$ and $w = 10°$ using Eq. (13) in the constant integrand approximation. It is obvious from the geometry in Figure 3 that the intensity distribution will be wider than the angle distribution, and that the index of refraction, which for the coatings is approximately 1.5, will also contribute to this widening. The graphs in Figure 4 for $w = 10°$ clearly illustrate the fact that the maximum reflectivity is not in the specular direction. The shapes of these graphs have changed from those in Ref. 8 because we have now taken into account the intensity changes at the interface and the difference in the element of solid angle.

Light Scattering Distribution Obtained from Topographic Maps

We generalize the method used to find the scattering distribution from topographic maps of dielectric coatings[13] to the scattering of light by flakes in coatings. We use the ray approximation in which we assume that a ray is incident in the given direction on each point of the map of the surface and is specularly reflected by a local tangent surface. We then count the number of reflected rays that end up inside a detector represented by a conical solid angle of given aperture about the scattering direction, weighted by the appropriate factors, that is,

$$I_j \Rightarrow I_j + (\cos \vartheta'_j / \cos \vartheta_j) T_{av} \gamma \tag{14}$$

The map we use does not represent a continuous surface but the surfaces of a number of flakes, possibly overlapping and separated by dark spaces. We have used two kinds of maps provided by the confocal microscope. The actual topographic map provides the values of the height where the intensity of the measured returned light is a maximum for a given location, which sometimes corresponds to weak stray light. The other map gives the maximum intensity as a function of location. To avoid the noise introduced by stray light measurements, we have masked the topographic map with the intensity map, that is, where the intensity is below a numerical threshold or cutoff value we have assigned a z-value of 0 to the corresponding location in the topographic map. The resulting intensity distributions are not very sensitive to the choice of this cutoff value in the vicinity of the minimum intensity in the map obtained by the microscope.

Since we do not have a continuous surface, we do not use a spline interpolation on the topographic map to obtain the local normal to the surface. We have used instead the method of the least-squares fit,[13] in which an approximation of the local tangent plane is determined by minimizing the sum of the squares of the distances of 24 neighboring points within a 5×5 square. We avoid some problems with the edges of the flakes or with bad data by dropping any rays that go to a point that includes values of $z = 0$ in the 5×5 square. We have not taken into account the special scattering by edges of conductors, which scatter light over greater angles. Furthermore, we have not attempted to identify the edges of overlapping flakes, which give rise to fictitious ridges that send rays into incorrect directions.

Here we take into account the refraction at the interface between the polymer coating and air, which change the direction of the ray and change the intensity by the average transmittance,

as explained above. We also take into account the varying area presented by the flake surface to the refracted incoming beam due to the inclination of the local normal.

Once we determine the local normal $\hat{n}$, we can follow the ray trajectory and obtain $\hat{k}'''$. If $\hat{r}_j$ is the *j*th position of the detector, the angle between the ray and the axis of the detector is given by

$$\cos\Delta = \hat{k}''' \cdot \hat{r}_j = \sin\theta''' \sin\vartheta_j \cos(\varphi''' - \varphi_j) + \cos\theta''' \cos\vartheta_j . \qquad (15)$$

If $\Delta < \alpha$, the ray enters the detector and we increase the corresponding intensity according to Eq. (14), where γ is the obliquity factor given by Eq. (2) and T_{av} is the average transmittance given by Eq. (10).

RESULTS AND DISCUSSION

The LSCM technique provides a non-destructive, powerful tool for characterizing the Al flakes in the coatings. Figure 5 shows the LSCM images of samples prepared under different spray conditions. The upper set of images represents the intensity profile in 2D projection and the lower set of images represents the topographic profile of the Al flakes distribution in a series of z-scan optical slices. The dark areas indicate the absence of Al flakes in the probed region. The shapes of the flakes appear to be platelet-like and surfaces of individual flakes are reasonably smooth. Slight variations in the sizes and shapes of flakes can also result in differences in appearance due to different spatial distributions of normals.[2]

To obtain the spatial orientation distribution of the flakes, we used up to 12 micrographs, measuring a total of 340 flakes for the 1-turn sample and 700 flakes for the 1.5-turn sample. Figure 6a shows the orientation (or inclination) distribution of the flakes in the 1.5-turn sample in terms of θ_x and θ_y, using the definition described in the theory section and illustrated in Figure 1. We used Eq. (6) to calculate the angle between the normal to the surface and the normal to the flake, θ_n, and the resulting distribution function, $p(\theta_n)$ is shown in Figure 6b. As mentioned previously, the intensity of the light scattered in a given direction is proportional to the total surface at a given angle. Thus, the determination of the distribution of the normals needs to take

into account the size of the flakes. The histograms in Figure 6 were obtained for the 1.5-turn sample and the data are sorted by 1^o per bin.

We then calculated the modified orientation distribution of flakes, $\tilde{p}(\theta_n)$, using Eq. (4). Figure 7 shows $\tilde{p}(\theta_n)$ for both 1-turn and 1.5-turn samples. The distributions appear to have a well-defined shape, but they are rather noisy, especially for the 1.5-turn sample. That of the 1-turn sample, not shown, is less noisy in spite of the smaller number of measurements. The process of obtaining these data is very laborious and it is unlikely that the statistics can be improved enough to obtain smooth histograms unless this process can be automated. The half-width of these histograms is about 3°.

We verified the isotropy of the samples by measuring the gonio-distribution of the reflectance for several position of the sample as it was rotated about the normal of the surface. The measurements indicated that the samples were isotropic at the scale of the 14-mm-diameter illuminated region.

The reflectance data are very similar in the specular peaks, since both samples contained the same polymer binder covered by a smooth clearcoat that does not significantly contribute to the scattering of light. Comparisons with the angular distribution of the light scattered by smooth epoxy coatings[13] and by coatings containing a thick layer of a top clearcoat suggest that the intensity in the specular peaks is caused by the reflection at the top surface of the coating and not by scattering due to the flakes. The half-width of about 1.5° corresponds to the aperture of the detector. In addition, we were able to confirm this hypothesis by a polarization scattering technique and distinguish different scattering sources and mechanisms of the scattered intensity.[14] The underlying off-specular (a few degrees away from the specular peak) reflectance is due to scattering from the subsurface microstructure — mostly from the reflections from the flakes.

Figure 8 shows the comparison between the measured reflectance data taken through the top clearcoat, including the additional clearcoat that was applied to obtain a smooth surface, and the reflectance calculated using a Gaussian modified angle distributions of flakes, $\tilde{p}(\theta_n)$, with half-widths w = 3° and w = 6°. The narrower Gaussian corresponds to the width of the histograms in Figure 7 and this width is clearly too small to explain the scattering distribution. The wider one provides a reasonable fit to the data about the specular region (excluding the specular

peak), with a discrepancy that becomes larger as the scattering angle moves away from the specular angle. This implies that the flake orientation (inclination) is not the only cause of the light scattering distribution. Some factors that would contribute to this discrepancy were ignored in the ray scattering model based on a flake orientation distribution. They include (1) additional scattering from the roughness of the flake surface, (2) incorrect shape and half-width of distribution function, (3) scattering due to multiple reflections from flakes, and (4) errors due to scattering from the edges of the flakes, especially from those that overlap.

To include the flake surface roughness contribution we have computed the scattered light distribution using a model similar to that used in Ref. 13. We assumed that rays are scattered specularly by a local tangent plane to the surface, as determined from maps obtained using the confocal microscope. In Figure 9 we compare the scattering intensity distributions obtained from the topographic maps using the ray approximation with the intensities measured by STARR. We show the scattering intensities for both samples and for angles of incidence of 30° and 60°. We have adjusted the vertical position of the calculated distributions to match the measured ones near the specular direction. The curves overlap quite well near the specular direction, and the discrepancies at angles furthest away from this direction can be due to the approximations involved in the model and to noise in the data. The logarithmic scale of the intensity axes exaggerates these differences. The calculated scattering distributions show a large peak in the specular direction that does not correspond to scattering by the top of the clearcoat, which was not included in the calculation. Instead, it is due to a large number of patches that have a normal in the vertical direction, apparently an effect of the interpolation algorithm used by the software of the confocal microscope.

CONCLUDING REMARKS

In this paper we have shown how data obtained from microscope images of a coating containing Al flakes can be used to compute light scattering distributions. These computed distributions are compared with measured ones to validate the approaches we have used.

The first approach singles out the effect of the flake orientation described by theoretical distributions of the angle the normal to the flake surface forms with the normal to the surface.

These distributions can be based on the actual distributions obtained from microscope images of the coating with the flakes, or a measured distribution can be used directly if it accurately represents the actual flake orientation distribution. An automated analysis to determine the images of the individual flakes in an image, requiring a robust edge-finding algorithm, is essential to obtaining good statistics in this process. The relationship between flake orientation distributions and reflectance can be used to evaluate the effects of a change in the flake distribution or, conversely, to estimate the distribution that can give rise to a measured reflectance curve. This approach assumes that the Al flakes are well approximated by smooth flat perfectly conducting surfaces. If the size and location distributions are included in the model, it may be possible to study the effects of multiple scattering by the flakes. The fact that the reflectance distribution obtained from a Gaussian with $w = 6°$ fits the data better than the one with $w = 3°$ indicates that factors other than the flake orientation, such as the roughness of the flake surface, contribute significantly to the light scattering and that the flakes used here cannot be considered flat perfectly conducting scatterrers.

The second approach involves the computation of the reflectance distribution using the topographic map directly. Some of the noise introduced by the measurement method of the confocal microscope had to be reduced by using the map of intensities provided by the instrument. This model is based on the reflection of the light ray by the local tangent plane to the surface of the flake, and thus takes into account the flake surface roughness. The computations described here show that the inclusion of the surface roughness of the flakes significantly improves the agreement between the computed and measured reflectance distributions. Computed reflectance values could be improved further by a better resolution of the images provided by the confocal microscope as well as better software to be used to control the instrument and to process the raw data. Our computations ignored the scattering by the edges of the flakes, multiple scattering, and the effects of the overlap of the flakes in the images.

Eventually, improved modeling methods, flake fabrication, and flake application techniques should lead to tools that can be used in the design and evaluation of metallic coating. These methods can also be extended to other types of media such as pigmented and pearlescent paints.

ACKNOWLEDGEMENTS

The authors would like to thank Dr. Thomas A. Germer for helpful discussions and for his polarization measurements. We also thank Michelle Clarke and Raphael Dutruc for helping with the microstructure characterization. This research is part of the Measurement Science for Optical Reflectance and Scattering Project at NIST.

Figure Captions

Figure 1: (a) LSCM image of intensity profile in a 2D projection and an extraction of an individual flake, (b) definition of the size and orientation of an individual flake used in this paper.

Figure 2: Geometry for the incident and scattering angles.

Figure 3: Ray trajectory for an oblique flake.

Figure 4: Calculated relative reflectance as a function of scattering angle. Solid lines: calculated normalized reflectance. Dashed lines: Gaussian flake orientation angular distribution functions centered at 0° with a half-width w, plotted about the specular direction.

Figure 5: LSCM images for two metallic pigmented samples (a) 1-turn and (b) 1.5-turn in 2D intensity projection (upper) and topographic (bottom) presentations.

Figure 6: Histograms for the 1.5-turn sample: (a) angular distribution of the flake orientation in the x- and y-directions, θ_x, θ_y, (b) distribution of the flake orientation with respect to the normal, θ_n.

Figure 7: Histograms of the modified flake orientation distribution functions, $\tilde{p}(\theta_n)$, for 1-turn and 1.5-turn samples.

Figure 8: Comparison between measured (dots) and calculated reflectance using a Gaussian flake orientation angular distribution of half-width angle w (solid lines: $w = 3^o$ and dashed lines: $w = 6^o$) of 1-turn and 1.5-turn samples for angles of incidence of 30° and 60°.

Figure 9: Comparison between measured (dots) and calculated (solid lines) reflectance of 1-turn and 1.5-turn samples for angles of incidence of 30° and 60°. The calculation uses the topographic and intensity maps measured with the confocal microscope.

REFERENCES

[1] Wicks, Z.W., Jones, F.N. Jr., Pappas, S.P., *Organic Coatings: Science and Technology*, John Wiley & Sons, Inc. (1992).

[2] McCamy, C.S., "Observation and Measurement of the Appearance of Metallic Materials, Part I. Macro Appearance & Part II. Micro Appearance" *Color Research and Application*, **21**, 292-304 (1996), **23**, 362-372 (1998).

[3] Rodrigues, A.B.J., "Color and Appearance Measurement of Metallic and Pearlescent Finishes," *ASTM Standardization News*, 68-72, October (1995).

[4] Tachi, K., Okuda, C., Suzuki, S., "Mechanism of Aluminum Flake Orientation in Metallic Topcoats," *Journal of Coatings Technology*, **62**, 43-50 (1990).

[5] Tachi, K., Okuda, C., "Color Variation of Automotive Metallic Finishes," *Journal of Coatings Technology,* **64**, 71-77 (1990).

[6] Wojtkowiak, J.J., "Effect of Film Viscosity on Aluminum Flake Orientation in Thermoplastic Acrylic Coatings," *Journal of Coatings Technology*, **51**, 111-116 (1979).

[7] Kettler, W.H., Richter, G., "Investigation on Topology of Platelet-Like Effect-Pigments in Automotive Surface-Coatings," *Progress in Organic Coatings*, **31**, 297-306 (1997).

[8] Sung, L.-P., Nadal, M.E., McKnight, M.E., Marx, E., Dutruc, R., and Laurenti, B., "Effect of Aluminum Flake Orientation on Coating Appearance," *FSCT/ICE 2001 Meeting Proceedings*.

[9] Corle, T.R., and Kino, G.S., *Confocal Scanning Optical Microscopy and Related Imaging Systems*, Academic Press (1996).

[10] Barnes, P.Y., Early, E.A., Parr, A.C., *Spectral Reflectance*, NIST Special Publication, 250-48 (1998).

[11] Barrick, D.E., "Rough Surface Scattering Based on the Specular Point Theory," *IEEE Trans. Antennas Propagat.* **16**, 449-454 (1968).

[12] Born, M. and Wolf, E., *Principles of Optics*, 6th Edition, p. 42, Pergamon (1980).

[13] McKnight, M.E., Marx, E., Nadal, M.E., Vorburger, T.V., Barnes, P.Y., Galler, M., "Measurements and Predictions of Light Scattering by Clear Epoxy Coatings," *Applied Optics*, **40**, 2159-2168 (2001).

[14] Germer, T.A., and Asmail, C.C., "Polarization of light scattered by microrough surfaces and subsurface defects," *J. Opt. Soc. Am. A*, **16**, 1326-1332 (1999).

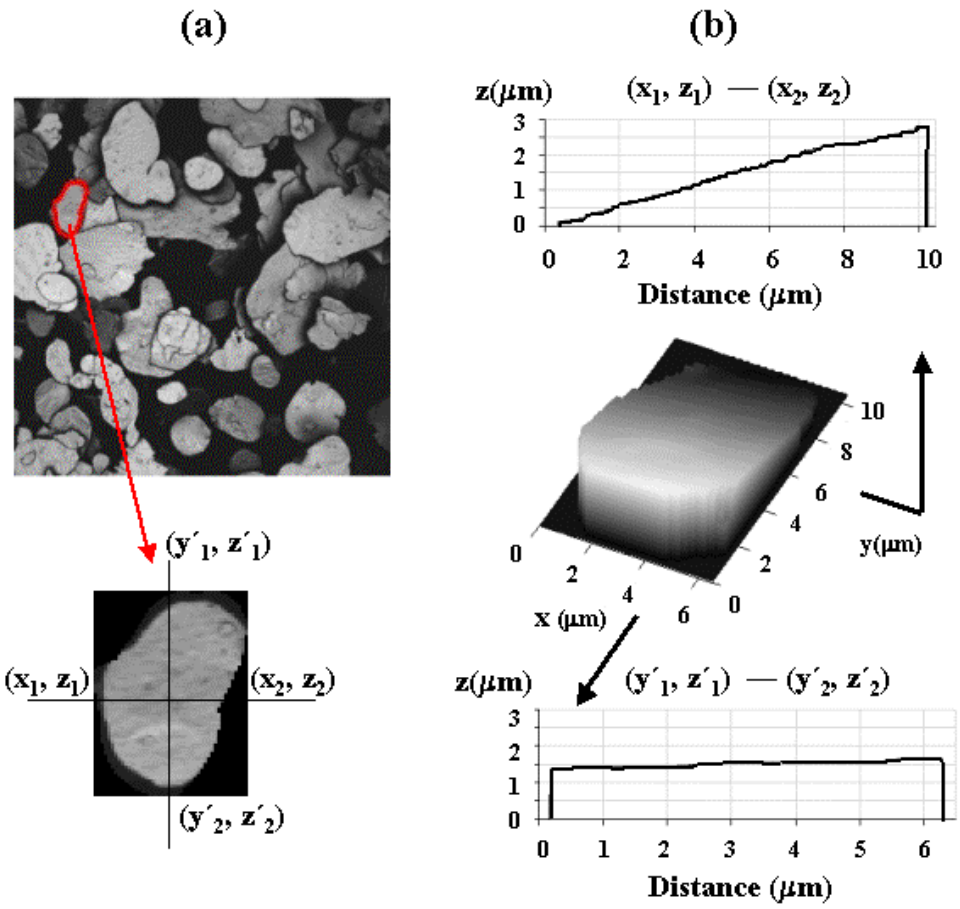

Figure 1: (a) LSCM image of intensity profile in a 2D projection and an extraction of an individual flake, (b) definition of the size and orientation of an individual flake used in this paper.

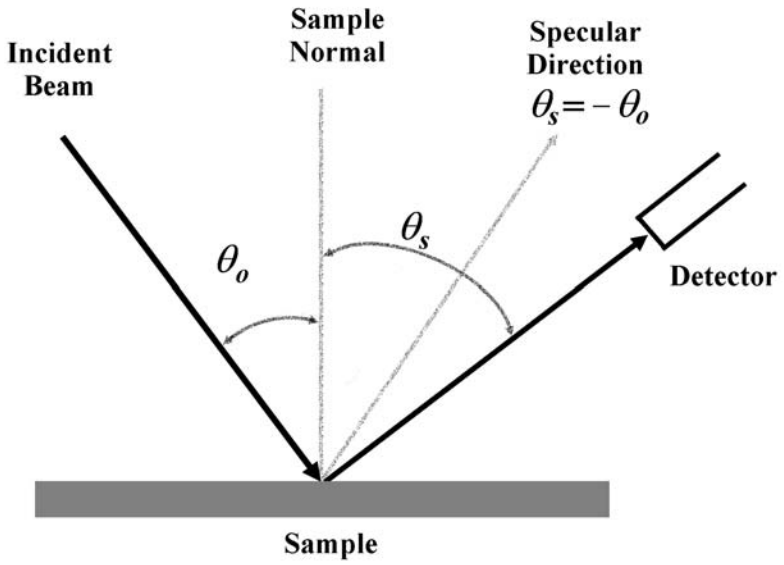

Figure 2: Geometry for the incident and scattering angles.

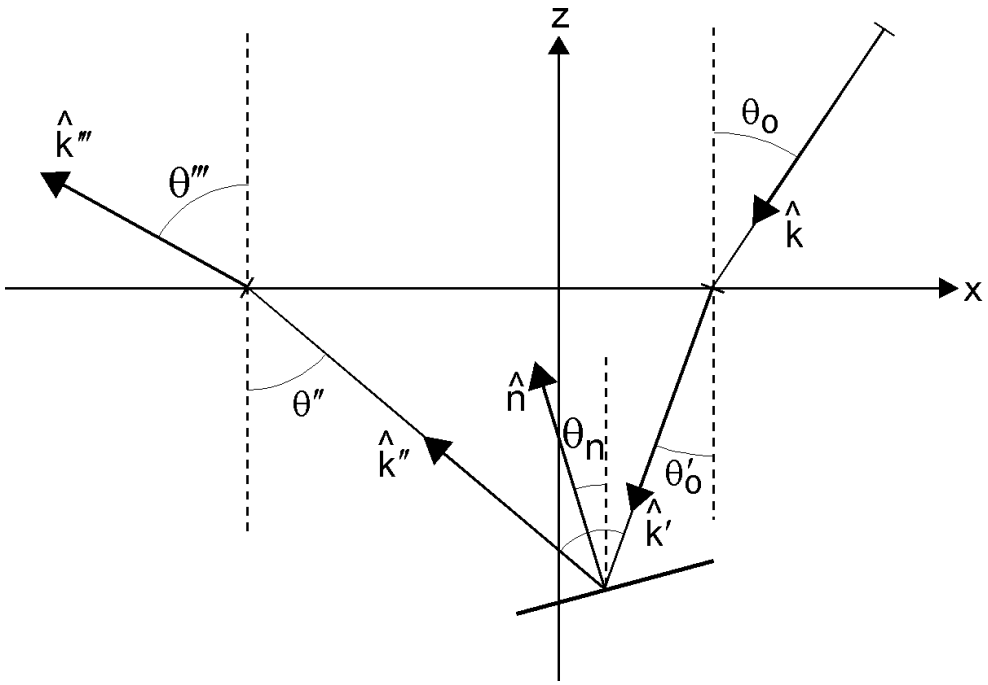

Figure 3: Ray trajectory for an oblique flake**.**

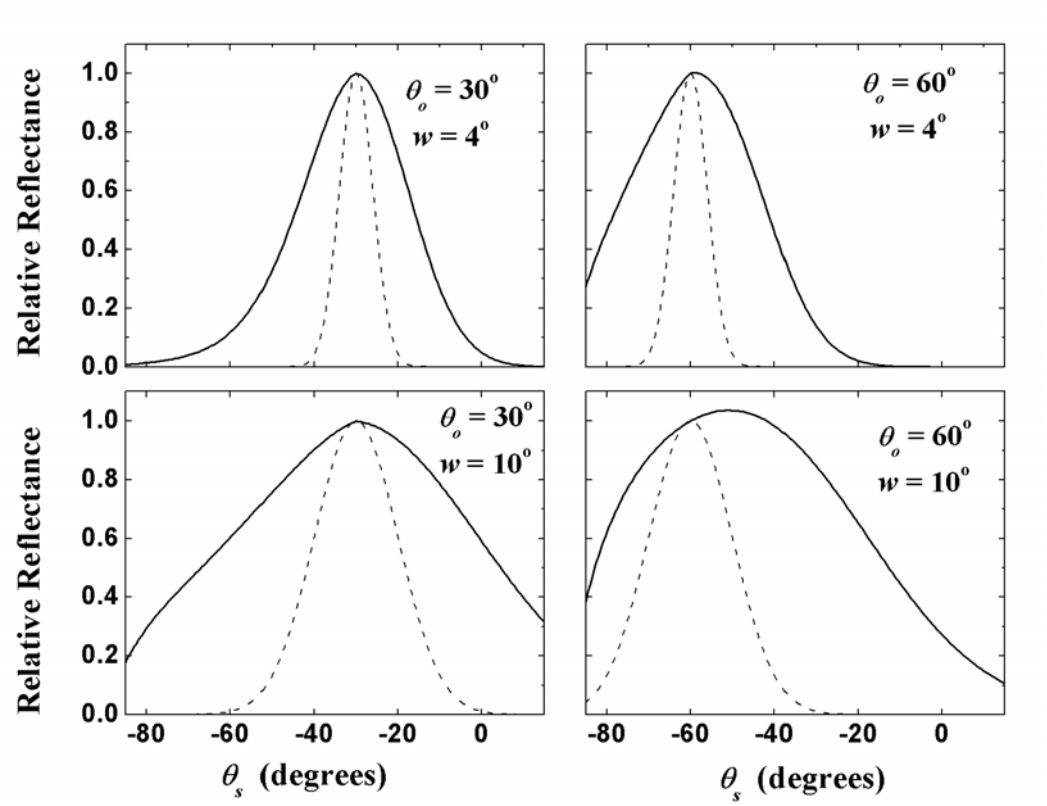

Figure 4: Calculated relative reflectance as a function of scattering angle. Solid lines: calculated normalized reflectance. Dashed lines: Gaussian flake orientation angular distribution functions centered at 0° with a half-width *w*, plotted about the specular direction.

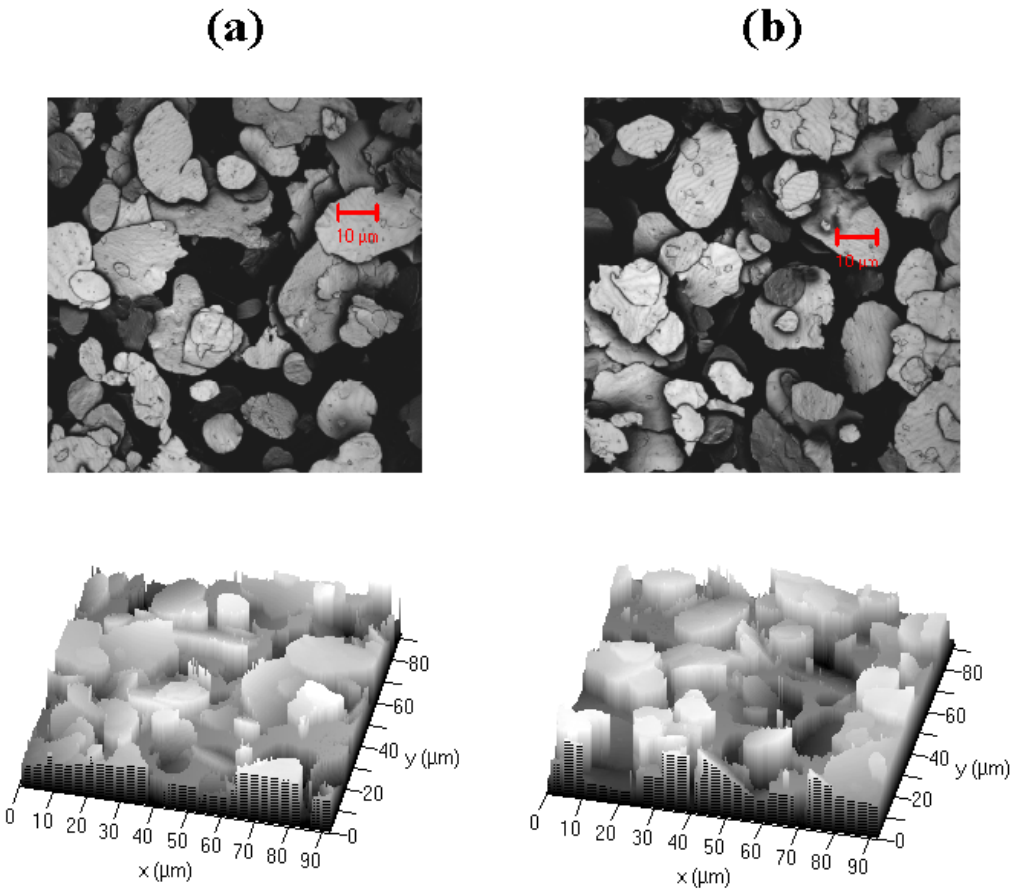

Figure 5: LSCM images for two metallic pigmented samples (a) 1-turn and (b) 1.5-turn in 2D intensity projection (upper) and topographic (bottom) presentations.

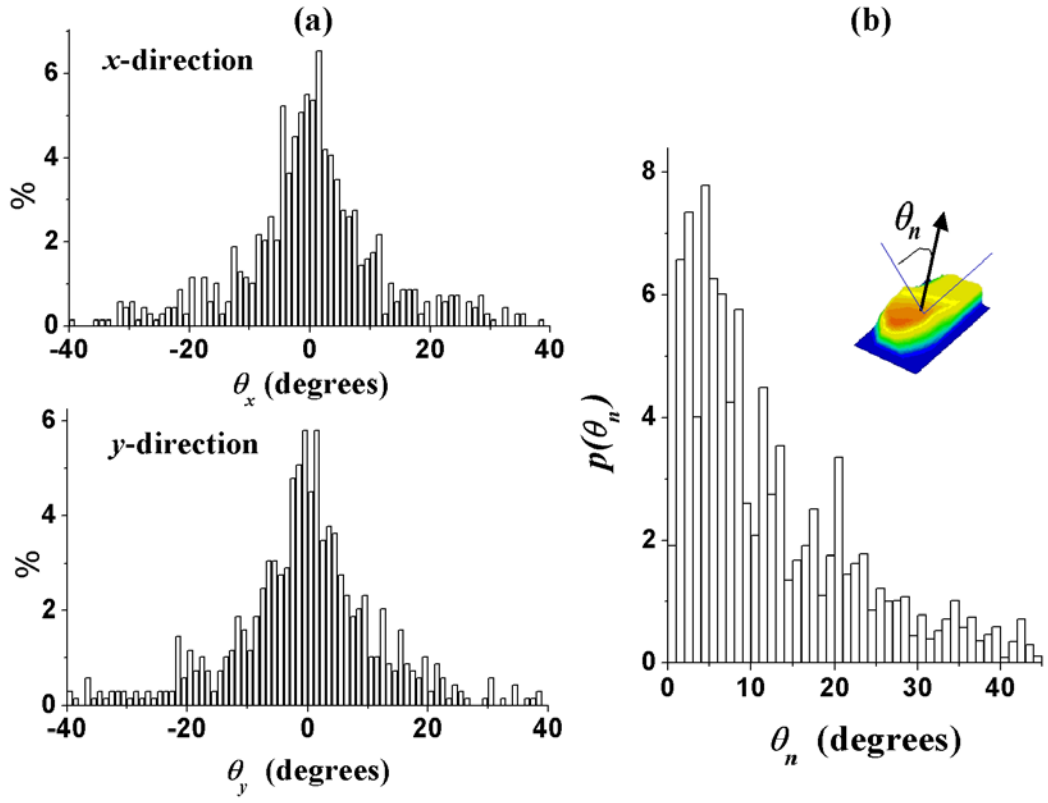

Figure 6: Histograms for the 1.5-turn sample: (a) angular distribution of the flake orientation in the *x*- and *y*-directions, θ_x, θ_y, (b) distribution of the flake orientation distribution function with respect to the normal, θ_n.

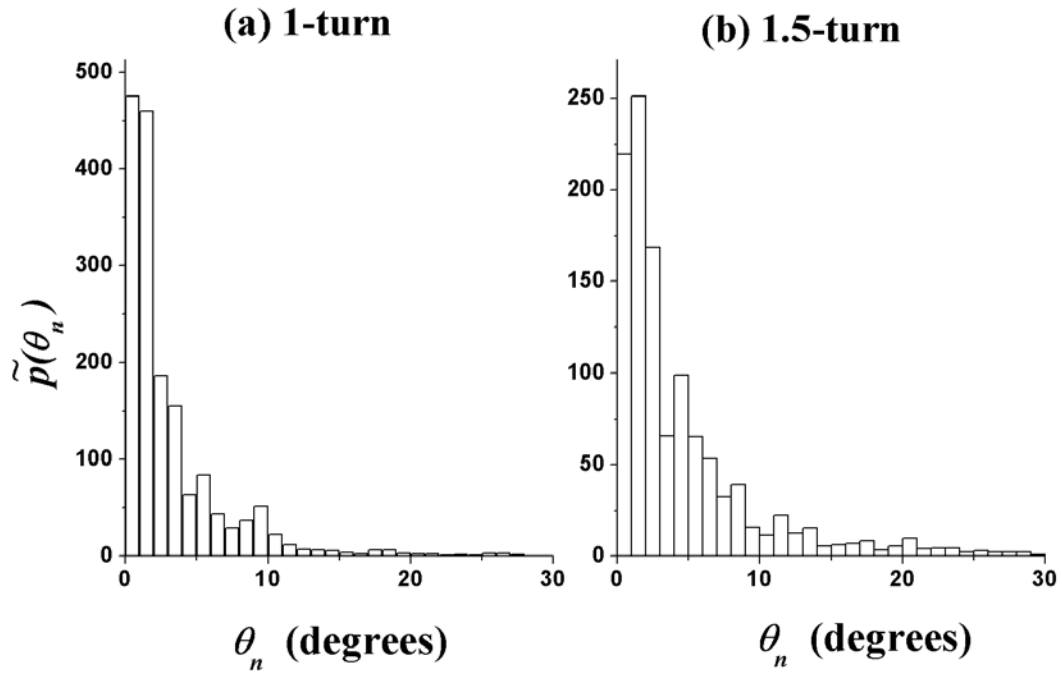

Figure 7: Histograms of the modified flake orientation distribution functions, $\tilde{p}(\theta_n)$, for 1-turn and 1.5-turn samples.

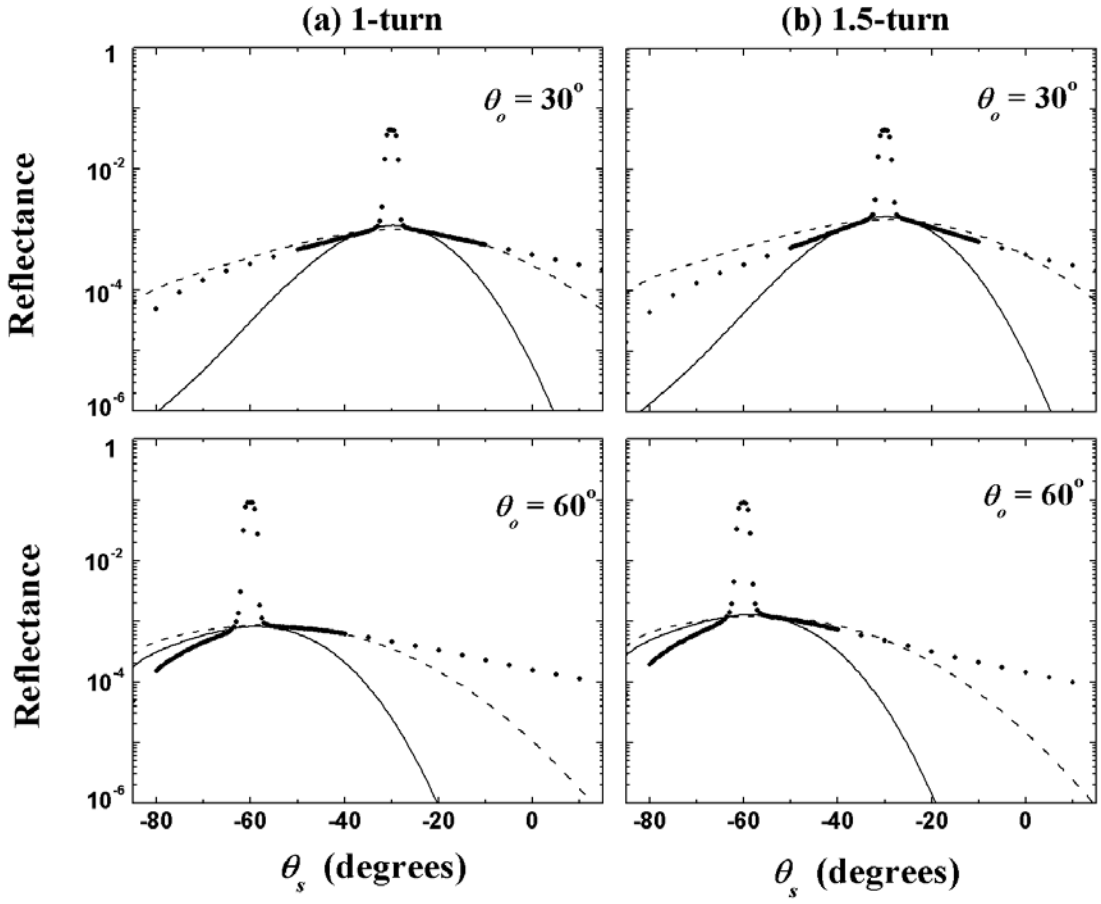

Figure 8:: Comparison between measured (dots) and calculated reflectance using a Gaussian flake orientation angular distribution of half-width angle w (solid lines: $w = 3^o$ and dashed lines: $w = 6^o$) of 1-turn and 1.5-turn samples for angles of incidence of 30° and 60°.

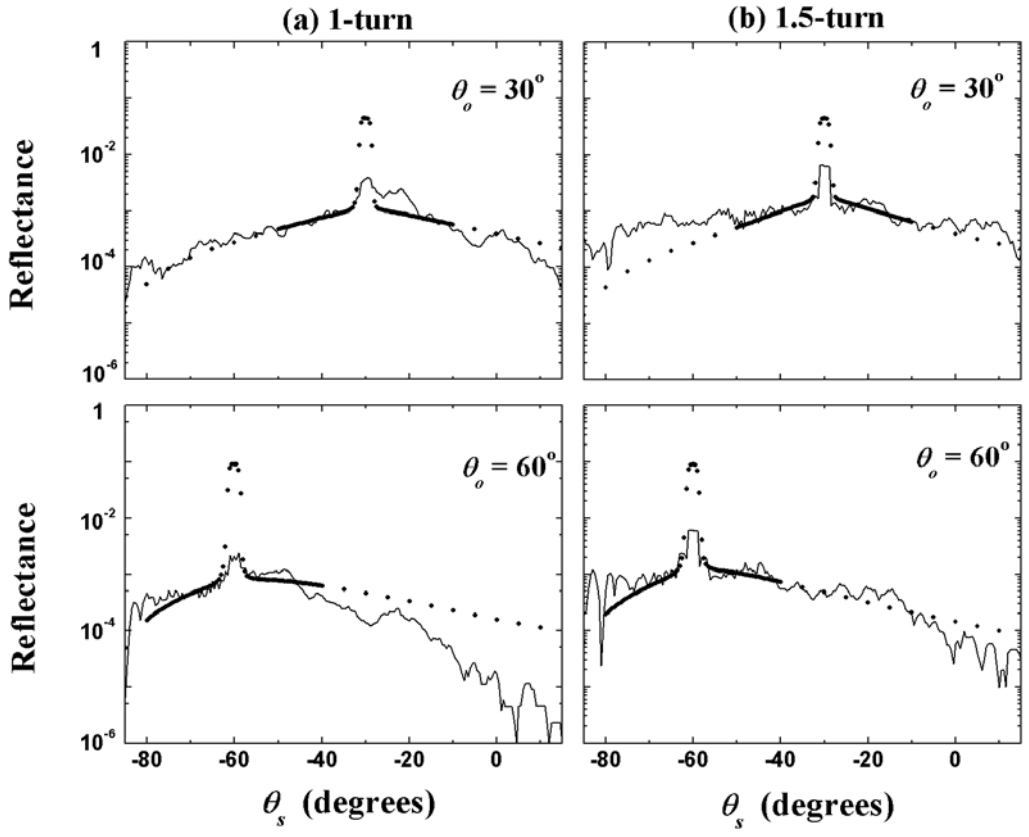

Figure 9: Comparison between measured (dots) and calculated (solid lines) reflectance of 1-turn and 1.5-turn samples for angles of incidence of 30° and 60°. The calculation uses the topographic and intensity maps measured with the confocal microscope.